Contents lists available at ScienceDirect

Arabian Journal of Chemistry

journal homepage: www.ksu.edu.sa

Study on preparation and properties of steel slag based composite gel for mine fire prevention and extinguishing

Tan Li [a,b], Hengze Zhao [a,b], Yipei Qi [a,b], Yu Zhang [a,b], Ye Li [a,b,c,*]

[a] School of Emergency Management and Safety Engineering, North China University of Science and Technology, Tangshan, Hebei 063210, China
[b] Tangshan Key Laboratory of Mine Safety and Emergency Management, Tangshan, Hebei 063210, China
[c] Hebei Key Laboratory of Mining Development and Safety Technology, Tangshan, Hebei 063210, China

ARTICLE INFO

Keywords:
Steel slag
Composite gel
Gelation mechanism
Fire-fighting performance
Flame retardant mechanism

ABSTRACT

A novel fire-preventing composite gel, mainly made from steel slag (SS) and silica fume (SF), was created for a coal mine's spontaneous combustion. The gelation mechanism of the steel slag-based composite gel (SSG) was investigated using X-ray diffraction (XRD), Fourier transform infrared spectroscopy (FTIR), and field emission scanning electron microscopy (SEM). The findings suggest that SSG is generated through the processes of hydration and geopolymerization involving SS and SF. And in the alkaline milieu of a 1.5 M water glass solution, SSG manifests enhanced strength and water retention capacities. Moreover, the fire prevention and extinguishing performance of the SSG was analyzed and verified using low-temperature oxidation, thermogravimetry, and low temperature nitrogen adsorption experiment (LTNA). The SSG has proven highly effective in suppressing spontaneous coal combustion by inhibiting CO production, raising the coal oxidation temperature, and reducing the contact area between oxygen and the coal body.

1. Introduction

Coal, being the primary energy source for industrial production and a non-renewable resource, holds immense value as a precious commodity (Huang et al., 2018, Li et al., 2019, Onifade et al., 2020). The spontaneous combustion in the goaf of coal mines poses a significant threat to mine safety, endangering the lives of workers and significantly depleting national energy resources. It is imperative that this issue be effectively prevented and controlled (Xu et al., 2020, Zhao et al., 2021).

Coal spontaneous combustion primarily consists of three conditions: the presence of coal with a natural propensity for self-ignition; sufficient oxygen exposure to generate heat; and an environment conducive to heat accumulation (Song et al., 2021). Therefore, the prevention and control of coal spontaneous combustion primarily focus on two strategies: isolating oxygen and promoting heat absorption and cooling. At present, the fire prevention and extinguishing materials designed to combat coal spontaneous combustion (Zhou et al., 2006, Wang et al., 2021, Huang et al., 2023) primarily encompass slurry, inert gas, inhibitors, foams and gels. However, the application of these fire prevention and extinguishing materials faces certain challenges, including the excessive fluidity of slurry during grouting, the susceptibility of inert gases to leakage, the low aging resistance of inhibitors, high cost, and the subpar foam stability (Slovák and Taraba 2012, Qin et al., 2016, Xue et al., 2020, Shi et al., 2021). In comparison to other fire prevention and extinguishing materials, gel is widely favored due to its exceptional capabilities in oxygen isolation, cooling, and plugging (Li et al., 2019, Guo et al., 2020). However, the currently most commonly employed inorganic silicic acid gel for fire prevention and extinguishing suffers from poor strength and is prone to water loss, leading to brittleness (Zhang et al., 2017).

In an effort to enhance the performance of gel and reduce costs, solid waste is being utilized to create a fire prevention and extinguishing gel material. Liang Wang (Wang et al., 2021) incorporated fly ash into konjac glucomannan (KGM) hydrogel, resulting in cross-linking between the fly ash and the three-dimensional KGM framework. This enhancement improved the water retention and permeability of the gel. Zhian Huang (Huang et al., 2018) developed an economical and environmentally friendly fly ash colloid fire prevention and extinguishing material by modifying the fly ash slurry with varying proportions of fly ash and suspending agents. Xiaofeng Ren (Ren et al., 2020) combined coal mine sludge with sodium carboxymethyl cellulose to create a novel sludge gel, aiming to reduce costs. This innovative approach not only

* Corresponding author at: School of Emergency Management and Safety Engineering, North China University of Science and Technology, Tangshan, Hebei 063210, China.
E-mail address: liye@ncst.edu.cn (Y. Li).

https://doi.org/10.1016/j.arabjc.2024.105966
Received 11 May 2024; Accepted 13 August 2024
Available online 14 August 2024

Table 1
Main Chemical Composition of SS and SF.

Raw material	Mass Fraction (%)				
	CaO	SiO_2	Al_2O_3	Fe_2O_3	MgO
SS	37.2	18.8	6.1	25.7	4.1
SF	1.0	90.5	0.7	2.2	1.6

enhanced the compressive strength and inhibition ability of the gel material but also facilitated the resource utilization of coal mine sludge. Although fly ash is the primary solid waste used for preparing anti-fire gels, there are various types of solid waste that possess gelling properties. These materials can also be employed to develop fire-fighting gels. In light of this, the current study aims to develop a novel, cost-effective and environmentally friendly composite gel material for mine fire prevention and extinguishing. To achieve these, steel slag (SS) can be utilized as the primary raw materials.

Steel slag, a by-product of the iron and steel industry, is a type of calcium-containing aluminosilicate solid waste. The mineral composition of steel slag mainly comprises dicalcium silicate (C_2S) and tricalcium silicate (C_3S) (Mengxiao et al., 2015, Wang et al., 2017, Jiang et al., 2018, Yu et al., 2023), which can undergo hydration reactions, leading to the formation of amorphous gel phases with the creation of three-dimensional structures composed of [SiO4] and [AlO4] tetrahedra (Guo et al., 2018, Zhuang and Wang 2021, Zhao et al., 2023). However, steel slag was mainly engineered for employment in construction filling as a replacement for cement, rather than being utilized as materials for mine fire prevention and suppression.

In this research, a novel fire prevention and extinguishing gel material was developed using 65 % steel slag as the primary raw material. To enhance the gelling properties of this material, silica fume (SF) (Popovics 1993, Richardson 1999, Jing et al., 2020) and a small amount of alumina are incorporated. The properties of the composite gel, including its gelling time, water retention capacity, thermal stability, and ability to inhibit coal spontaneous combustion, were thoroughly examined. Moreover, an exhaustive elucidation of the gelling mechanism and flame-retardant mechanism inherent to the composite gel was furnished. This study outcomes augment the high-value application of steel slag in gel materials for mine fire prevention and suppression, effectively mitigating risks linked to coal extraction. This is of paramount importance to the safety of coal mining operations.

2. Preparation and characterization

2.1. Raw materials

Steel slag (SS) and silica fume (SF) were utilized as the primary materials for developing a mine fire extinguishing gel. The steel slag was sourced from Tangshan Steel Plant and had a medium alkalinity of 1.94. Silica fume, supplied by Hefei Anshan Fluid Technology Co. Ltd., is primarily composed of SiO_2. Table 1 displays the primary chemical compositions of SS and SF, as identified by X-ray fluorescence spectrometer (XRF, ZSX Primus II, Japan). Alumina (AR, Shanghai) was incorporated as a supplementary aluminum source. Water glass (modulus M=3.3, Na_2O=8.3 wt%, SiO_2 = 26.5 wt%, Qingdao) and sodium hydroxide (Shanghai) were used as the alkali activator. The modulus "M" represents the molar ratio of silicon dioxide to alkali metal oxide. $NaHCO_3$ (Shanghai) was employed as a coagulant.

2.2. Preparation of gel

The gel preparation process is illustrated in Fig. 1. Steel slag, silica fume, and alumina are mixed in a specific ratio of 50:17:10 to achieve a calcium-silicon ratio of 0.8 and a calcium-aluminum ratio of 1.4. To prepare the gel, 100 g of deionized water is combined with 9 % of 1.5 M water glass to form a mixed solution. The 1.5 M water glass is prepared by mixing 3.3 M water glass with sodium hydroxide in a ratio of 100:13.1. This solution is then poured into 50 % of the mixed powder and thoroughly stirred. Subsequently, 6.25 % of $NaHCO_3$ is added to the mixture and stirred again before pouring it into the mold and allowing it to gel. (All percentages mentioned are based on the weight of water.).

3. Performance testing experiment

3.1. Composition and structure

Prior to the testing experiment, the gel samples were subjected to vacuum drying in an oven at 40 °C for a duration of 24 h (Zhou et al., 2006, Shi et al., 2021). Subsequently, the mineral phases present in the SSG were characterized using an X-ray polycrystalline diffractometer within a 2θ angle range of 5° to 65° (XRD, Empyrean, Holland). The functional groups present in the SSG were identified through Fourier transform infrared spectroscopy within the wavenumber range of 400

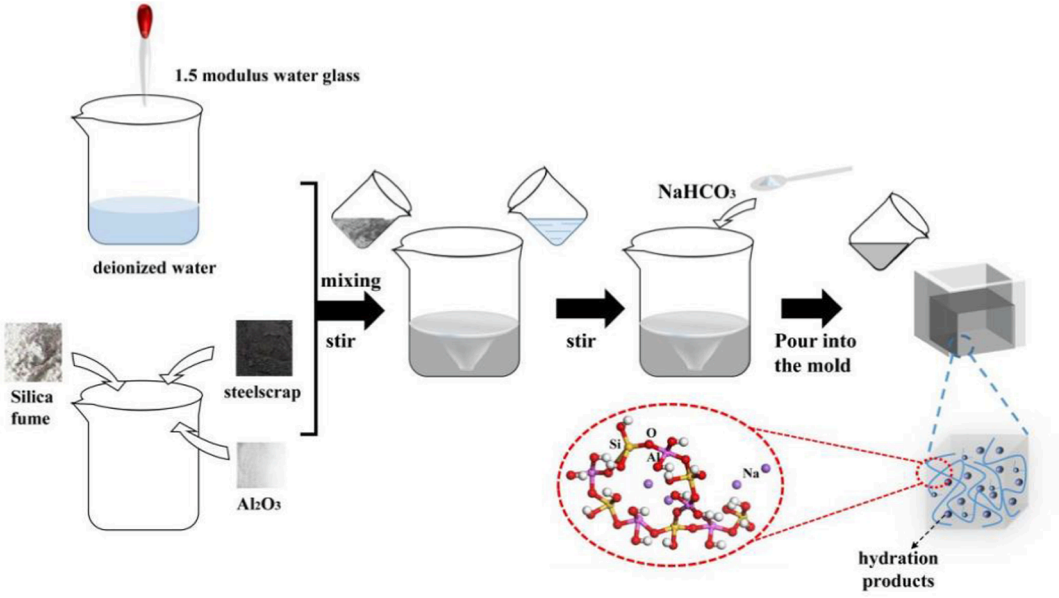

Fig. 1. Preparation of Gel.

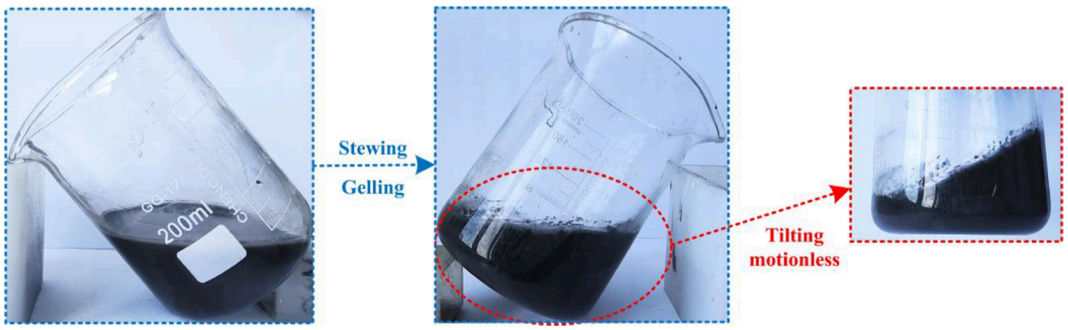

Fig. 2. Determination of gelation time.

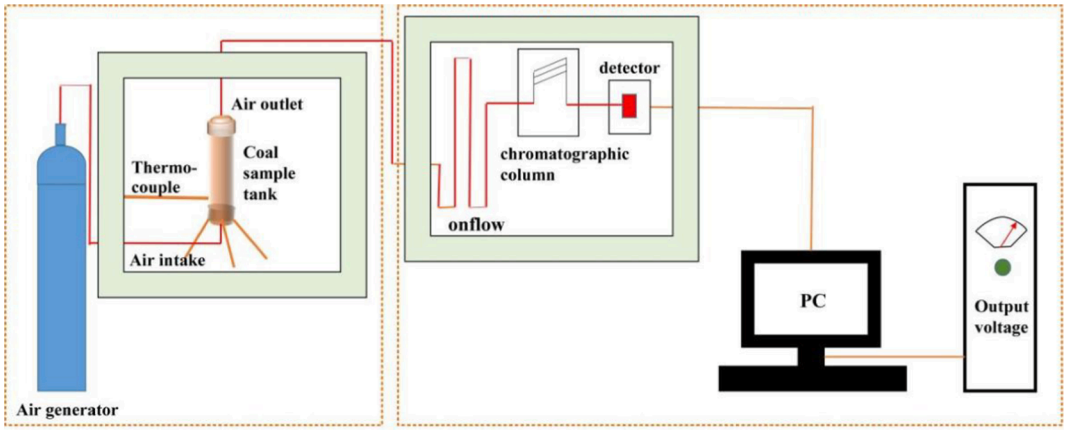

Fig. 3. Low temperature oxidation system.

cm^{-1} to 4000 cm^{-1} (FT-IR, VERTEX70, America).

The gel samples were examined before and after the fire extinguishing process using a field emission scanning electron microscope (SEM, HITACHI SU5000, Japan). Before the experiment, the sample was freeze-dried at −40 °C for a duration of 24 h to ensure the preservation of the gel structure's integrity. (Wang et al., 2021).

3.2. Determination of gelation time

As illustrated in Fig. 2, the gelation time of the gel material was determined using the test tube method. After the mixture had been prepared, begin timing. Tilt the beaker at a 45° angle and observe if the slurry continues to flow or if it remains stationary. This indicates the gelation time of the material. The above operation should be repeated three times to ensure accuracy and consistency. The average value obtained from these three trials should then be taken as the final result.

3.3. Water loss rate

Document the initial mass (m_0) of water employed in the preparation of SSG. Subsequently, place the sample in a vacuum drying oven at a constant temperature of 100 ℃ and weigh it at hourly intervals for a period of 11 h. Calculate the hourly water loss rate of the gel according to the following formula (Li et al., 2019, Ren et al., 2020). The aforementioned process is repeated thrice, and the average value is computed.

$$\text{Water loss rate} = \frac{m_i - m_{i-1}}{m_0}$$

m_0—initial mass, g;
m_i—After i hours, peel the beaker and weigh the mass, g;
m_{i-1}—After i-1 h, peel the beaker and weigh the mass, g.

3.4. Low temperature oxidation experiment

3.4.1. Experiment system

As illustrated in Fig. 3, the inhibition effect of SSG on coal spontaneous combustion was assessed using a temperature program-gas chromatography linkage device, which primarily comprises the gas generated by the heating furnace and the gas components detected by gas chromatography. The sample was placed in a coal sample tank and heated from 30 to 260 °C. A thermocouple in the coal sample tank detects the temperature of the coal and the furnace. The change in temperature at the crossing point could be displayed, and a chromatograph was used to analyze the composition and content of gas generated during the temperature rise process.

3.4.2. Coal self-combustion inhibition rate

The coal powders used in the study were sourced from the gas coal (GC) of Tangshan Donghuantuo Mine and the fat coal (FC) of Tangshan Qianjiaying Mine. The coal powders were crushed and sieved to a size range of 20–60 mesh, followed by vacuum drying at 40 °C for 12 h. Two 40 g samples of each coal type were weighed, and one of them was mixed with a gel in a ratio of 1:1 to create a gel/coal sample mixture. Four samples (GC, GC+SSG, FC, FC+SSG) were analyzed using the temperature program-gas chromatography linkage device. The CO index gas, which is universally acknowledged, serves as an early warning signal for coal's propensity to combust spontaneously (Mengxiao et al., 2015, Wang et al., 2021). Additionally, the inhibitory effects of FC and GC on this spontaneous coal combustion are determined through calculation.

$$\text{Coal self - combustion inhibition rate} = \frac{c_{i1} - c_{i2}}{c_{i1}} \times 100\%$$

c_{i1}—The concentration of CO produced by raw coal at temperature i,

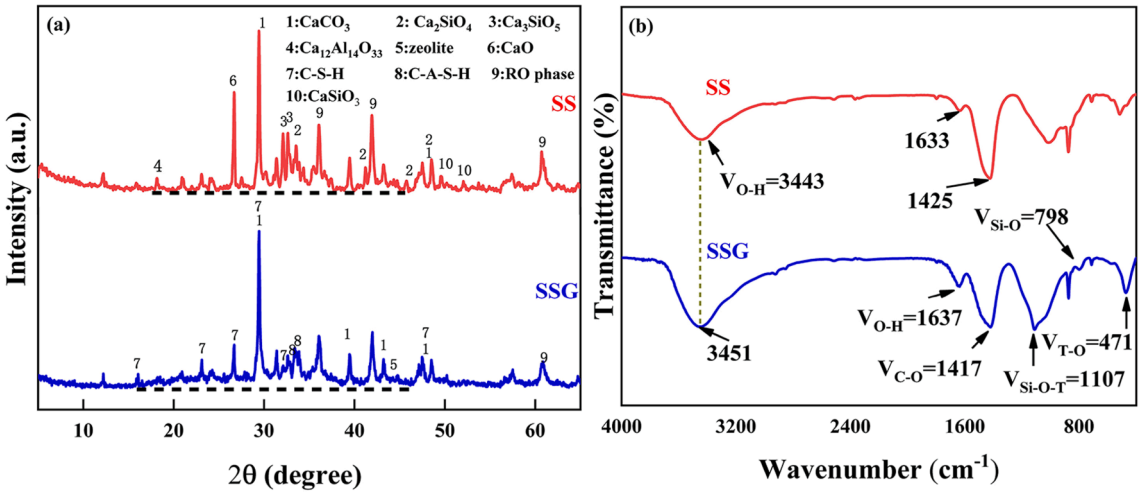

Fig. 4. XRD and FTIR spectra of SS and SSG.

ppm;

c_{i2}—The concentration of CO produced by the gel/coal sample at temperature i, ppm.

3.5. Analysis of thermal stability

Two samples, labeled FC and GC, were placed in a vacuum drying oven and maintained at a temperature of 40 °C for a duration of 24 h. The thermal stability of the four samples (dried FC and GC, bulk FC+SSG and GC+SSG) was then studied using a simultaneous thermal analyzer (TG-DTG, STA200, Japan), which heated the samples from 20 °C to 800 °C at a rate of 10 °C/min in air with a flow rate of 50 mL/min.

3.6. Low temperature nitrogen adsorption experiment (LTNA)

The JW-BK112 specific surface area and pore size analyzer was used to measure the specific surface area of the samples. Four samples (GC, GC+SSG, FC, FC+SSG) were dried in vacuum, and 2.5 g of each sample within the 20–60 mesh range was selected for heat treatment to desorb gas. The samples were then repeatedly adsorbed in a liquid nitrogen environment to calculate the specific surface area. This analysis allowed for the examination of changes in the pore structure and contact area of

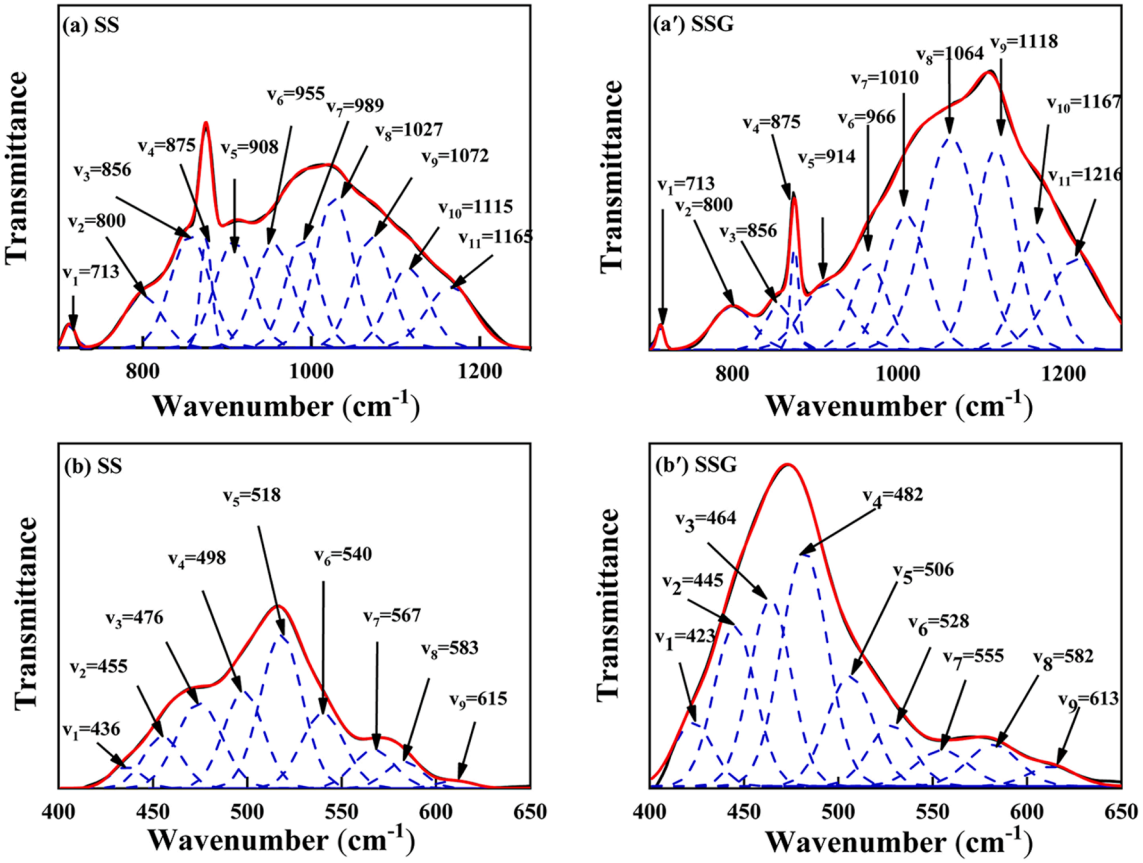

Fig. 5. FTIR spectra of SS and SSG at different wavenumbers (a) SS 700–1260 cm^{-1}; (a′) SSG 700–1260 cm^{-1}; (b) SS 400–650 cm^{-1}; (b′) SSG 400–650 cm^{-1}.

Table 2
Characteristic peak assignment at 700–1260 cm^{-1}.

Number	Characteristic peak wavenumber (cm^{-1})	Characteristic peak assignment
V_1	713.0	C-O
V_2	800.0	Si-O (C_2S)
V_3	856.0	Si-O (C_2S)
V_4	875.0	C-O
V_5 / V_6 / V_7	908.0 / 955.0 / 989.0	Si-O-Si (C-S-H)
V_8 / V_9 / V_{10} / V_{11}	1027.0 / 1072.0 / 1115.0 / 1165.0	Si-O-T (Si/Al)

Table 3
Characteristic peak assignment at 400–650 cm^{-1}.

Number	Characteristic peak wavenumber (cm^{-1})	Characteristic peak assignment
V_1	436.0	(Si/Al) T-O
V_2	455.0	Si-O (C_3S)
V_3	476.0	(Si/Al) T-O
V_4	498.0	Si-O (C_2S)
V_5 / V_7 / V_8	518.0 / 567.0 / 583.0	(Si/Al) T-O ($Ca_{12}Al_{14}O_{33}$)
V_6 / V_9	540.0 / 615.0	Si-O-Si

the coal samples under the influence of the gel.

4. Results and discussion

4.1. Gelling mechanism

4.1.1. XRD and FTIR

The XRD diagrams of SS and SSG are presented in Fig. 4(a). The primary crystalline phases in SS are calcite ($CaCO_3$), quicklime (CaO), tricalcium silicate (Ca_3SiO_5), dicalcium silicate (Ca_2SiO_4), calcium silicate ($CaSiO_3$), dodecacalcium heptaluminate ($Ca_{12}Al_{14}O_{33}$), and RO phase. Upon the conversion of SS into SSG, a noticeable alteration in the mineral phase occurred. The formation of several new crystalline phases, including Calcium Silicate Hydrate (C-S-H), Calcium Aluminum Silicate Hydrate (C-A-S-H), and zeolite, has been observed. Furthermore, a noticeable swelling is observed between 20° and 40°, suggesting the formation of an amorphous gel phase. During this process, the peak intensities of CaO, Ca_3SiO_5 (C_3S), Ca_2SiO_4 (C_2S), $CaSiO_3$, $Ca_{12}Al_{14}O_{33}$, and RO phase were noticeably reduced, indicating their participation in the phase transition.

The alterations in functional groups of SS and SSG are illustrated in Fig. 4(b). The vibration peaks of –OH can be observed at 3443 cm^{-1} and 1633 cm^{-1} in SS (Mengxiao et al., 2015, Ren et al., 2020, Wang et al., 2021). During the transformation of SS into SSG, the hydroxyl peaks shift to 3451 cm^{-1} and 1637 cm^{-1} respectively and their intensity and area increase. This suggests that more free water is present in the structure, which can be beneficial for fire prevention. In SS, the peak at 1425 cm^{-1} corresponds to the bending vibration peak of CO_3^{2-} (Tang et al., 2024), which is derived from the calcite. In SSG, the absorption peak of carbonate weakens and shifts to a lower wave number, suggesting a minor decomposition of calcite. This observation is consistent with the XRD results. The most prominent vibration bands are observed between 700–1260 cm^{-1} and 400–650 cm^{-1}, which correspond to the asymmetric stretching vibration of the Si-O-T (Si, Al) bond and the bending vibration of (Si, Al) T-O, respectively (Duan et al., 2018, Liu et al., 2021). These bands are associated with the formation of the amorphous gel (C-(A)-S-H) through the hydration reaction and geopolymerization. Consequently, the peaks in the range of 700–1260 cm^{-1} and 400–650 cm^{-1} are analyzed to investigate the gelation mechanism.

Fig. 5 illustrates the infrared peak splitting results of SS and SSG in the range of 700–1260 cm^{-1} and 400–650 cm^{-1}. The assignment of specific peaks is also summarized in Tables 2 and 3. In the range of 700–1260 cm^{-1}, as SS transforms into SSG, the majority of the absorption peaks shift towards higher wave numbers. This suggests that the polymerization degree of the Si-O-T bond increases, and more three-dimensional gel networks appear. This observation is consistent with the peak packet of amorphous phase shown in the XRD results. Moreover, the intensity of C-O absorption peak at 713 cm^{-1} and 875 cm^{-1} decreases, suggesting the decomposition of $CaCO_3$ (Sang et al., 2024, Tang et al., 2024). The Si-O absorption peaks at 800 cm^{-1} and 856 cm^{-1} significantly decrease in area. This can be attributed to the consumption of Ca_2SiO_4 during the gel reaction, which is consistent with the decrease of their crystal phases in XRD results (Liu et al., 2023). Additionally, within the 400–650 cm^{-1} range, the absorption peaks exhibit a negative shift. The primary factors contributing to this outcome are discussed below. As the gel phase forms, a large number of [SiO3] structures transform into [SiO4] structures, and some [SiO2] structures are also generated (Song et al., 2020, Liu et al., 2021, Zhang et al., 2023). At this stage, the degree of polymerization for the Si-O bond is elevated, resulting in an increase in the peak area, suggesting the formation of new gel phase. Meanwhile, the replacement of Si-O bonds with Al-O bonds results in the formation of Si-O-Al bonds, causing a shift in the absorption peak position towards the negative direction (Liu et al., 2019, Zhang et al., 2023). The peaks corresponding to Si-O/Al-O bonds at 518 cm^{-1} 、 567 $cm^{-1}$and 583 cm^{-1} exhibit a reduction in peak area and a negative shift in wavenumber, indicating the decomposition of $Ca_{12}Al_{14}O_{33}$ (Tang et al., 2024). Moreover, The negative shift of the peaks at 455 cm^{-1} and 498 cm^{-1} corresponds to the decomposition of Ca_2SiO_4 and Ca_3SiO_5 (Tang et al., 2024). And the negative shift of the

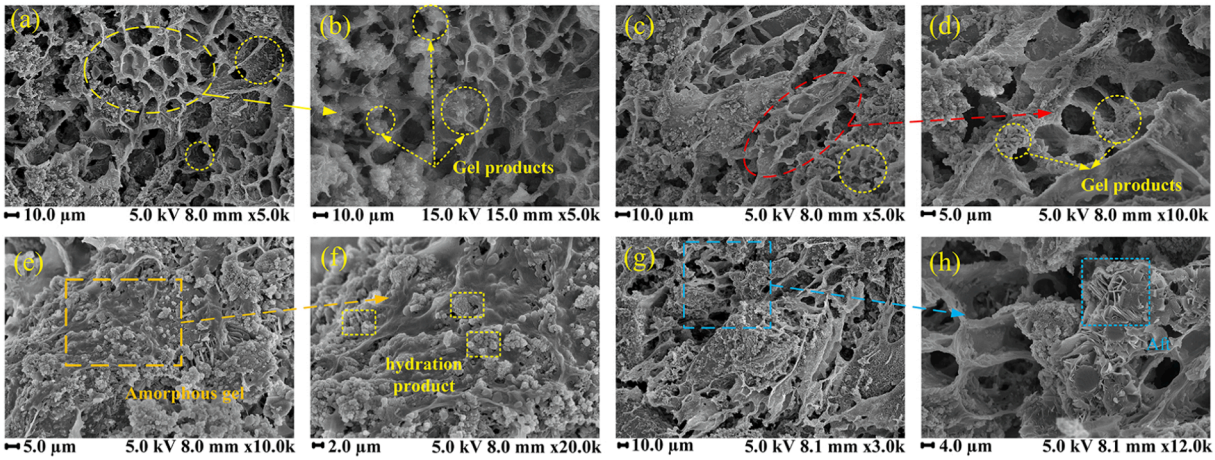

Fig. 6. SEM microstructure images of SSG.

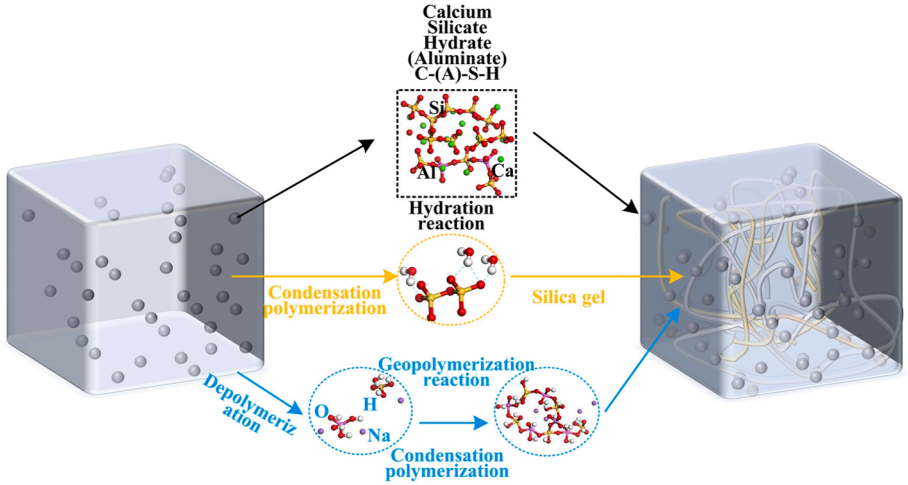

Fig. 7. Gelation mechanism of SSG.

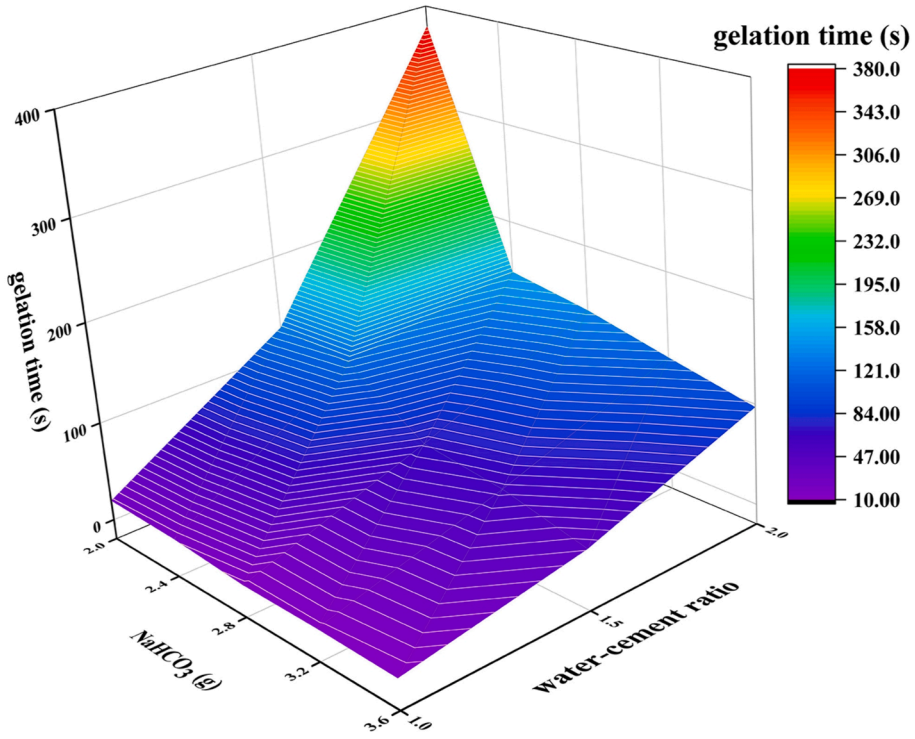

Fig. 8. Influence of $NaHCO_3$ dosage on gel time at different water cement ratios.

peaks at 540 cm^{-1} and 615 cm^{-1} corresponds to the decomposition of silicates and aluminates in SS (Wang et al., 2014, Tang et al., 2024). Therefore, the Si-O and Al-O bonds break and dissociate into free monomers. The Ca^{2+} in steel slag combines with these free monomers to form C-(A)-S-H.

4.1.2. Microstructure

Fig. 6 presents the microstructure characterization of SSG through scanning electron microscopy. During the freeze-drying process, water evaporates from the densely packed pores, resulting in the formation of some adhesive three-dimensional network structures. In addition, gel products of varying shapes and sizes can be observed attached to the wall of the pores (Fig. 6 (b)). This enhances the network structure's adhesion, consequently increasing its water absorption capacity. In Fig. 6 (e) and (f), a substantial amount of amorphous gels can be observed encapsulating compounded steel slag particles and some hydration products. These gels fill the pores, resulting in a more compact and uniform structure with enhanced strength and reduced susceptibility to cracking (Liu and Guo 2018, Guo and Pan 2020).

4.1.3. Gelation mechanism of SSG

Fig. 7 depicts the gelation mechanism of SSG. Under adequate alkaline conditions, the hydration of C_2S, C_3S, and $Ca_{12}Al_{14}O_{33}$ in complex steel slag leads to the formation of C-S-H and a minor amount of C-(A)-S-H (Liu et al., 2023, Samchenko and Korshunov 2023). The amorphous polymer resulting from the hydration reaction adheres to the silica gel and geopolymeric gel network (Bernal et al., 2012), which is formed by the polycondensation of silicate and aluminate molecules. This product fills voids, enhances strength, and ultimately culminates in the formation of the SSG composite gel.

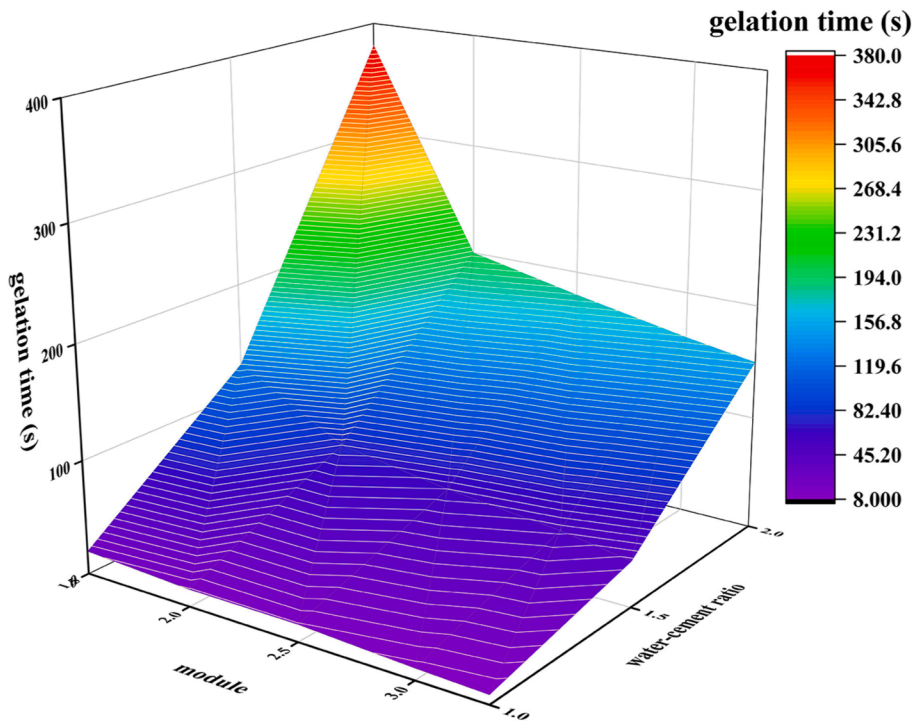

Fig. 9. Influence of modulus on gel time at different water cement ratios.

4.2. Gel time

The addition of $NaHCO_3$ as a coagulant was investigated, and its impact on the gel time at various water-cement ratios is illustrated in Fig. 8. As the concentration of $NaHCO_3$ increases, there is a significant reduction in gel time. In the solution, $NaHCO_3$ undergoes dissociation to release H^+ ions and reacts with water glass to form a silicate gel (Huang et al., 2018, Huang et al., 2023), which can enhance the viscosity of the solution and augment the stability of the compounded steel slag within the solution. As the addition amount of $NaHCO_3$ increases, more silicate gel is formed. Upon further increasing the viscosity of the solution, the mobility of the substances within it decelerates. The silica and aluminum tetrahedrons, liberated from steel slag and silica fume under the influence of alkaline activator, rapidly engage in a reaction to form a gel structure within a confined area. This accelerated reaction consequently leads to a diminished gelation time.

Fig. 9 illustrates the impact of water glass modulus on gel time at varying water cement ratios. At a constant water-cement ratio, an increase in water glass modulus leads to a reduction in gel time. Under typical conditions, elevating the sodium silicate modulus diminishes the alkalinity of the slurry, consequently slowing down the generation rate of silica tetrahedron and aluminum tetrahedron, thereby impacting the gel reaction. However, upon increasing the water glass modulus, there is a notable rise in the slurry's viscosity. Furthermore, a significant quantity of silicate found within the slurry can swiftly react with $NaHCO_3$, resulting in the generation of a large amount of silicate gel, which further heightens the viscosity of the slurry. Despite the low production rate of silicon oxide tetrahedron and aluminum oxide tetrahedron, their reaction speed is faster, leading to a shorter gel time.

Moreover, augmenting the water content in the slurry results in an extended gel time. This phenomenon is chiefly attributed to two factors. The one is that the diminished alkalinity of the slurry, which arises from the increased water quantity. Consequently, the reactivity of the compounded steel slag gets impeded, necessitating a longer reaction duration for gelation to occur. Another one is that raising the water content precipitates a decline in the slurry's viscosity, which, in turn, decelerates the gel reaction rate.

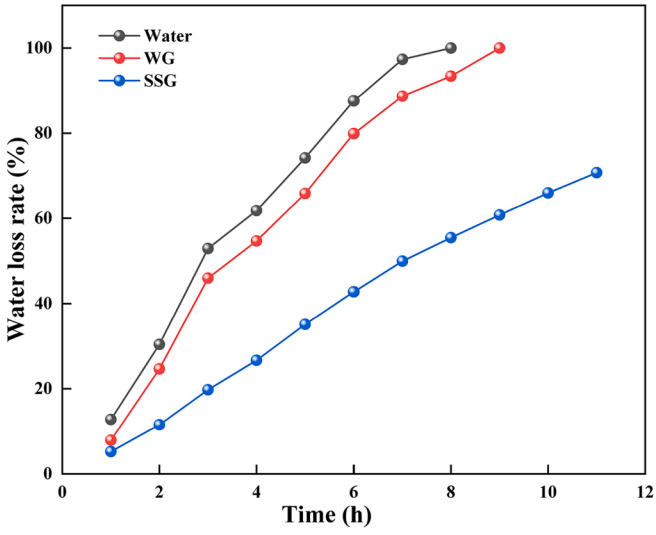

Fig. 10. Water loss rate of different materials.

4.3. Water loss rate

As illustrated in Fig. 10, the water loss rates of water, water glass gel, and SSG at a constant temperature of 100 °C for 11 h are depicted. It is evident that the water loss rates of water and water glass gel reach 100 % at 8 h and 9 h, respectively. In contrast, the water loss rate of SSG remains significantly lower, with a value of 70.75 % even after being subjected to constant temperature conditions for 11 h. The unique three-dimensional network gel structure of SSG possesses a higher density, effectively trapping water molecules within the grid and thereby preventing moisture loss. This characteristic contributes to the superior water retention properties of SSG compared to traditional water glass gels.

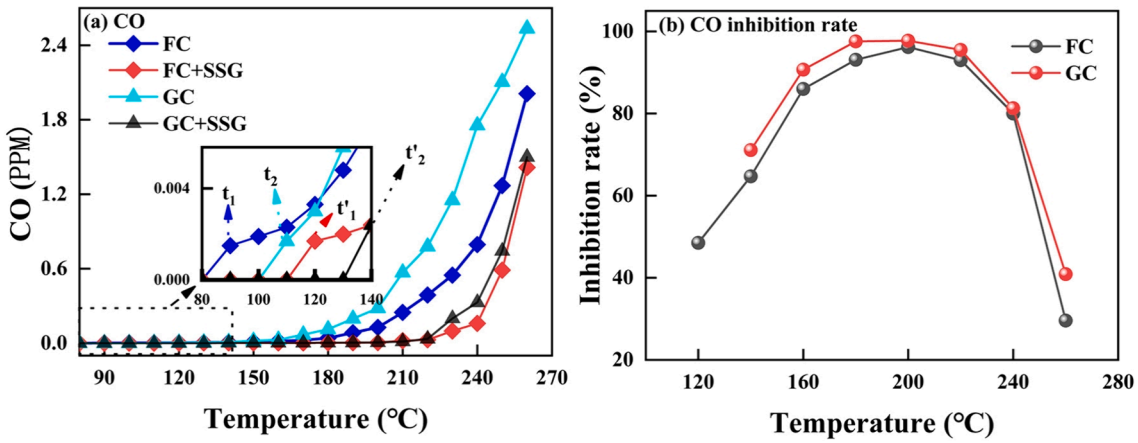

Fig. 11. (a) CO emission of FC and GC before and after SSG treatment; (b) Oxidation inhibition rate of FC and GC treated by SSG.

Table 4
Changes in Crossover Temperature of GC and FC.

Sample	Crossover Temperature (℃)	Time to reach crossover temperature (min)
FC	207.8	176.0
FC+SSG	257.7	221.0
GC	198.9	166.0
GC+SSG	251.9	217.0

Note: The crossover temperature refers to the specific temperature at which the coal temperature equals the furnace temperature.

4.4. Inhibition analysis

Fig. 11(a) illustrates the changes in CO concentration resulting from the oxidation and heating of FC and GC before and after undergoing SSG treatment. Fig. 11(a) shows that t_1 and t_1' are the temperature points at which FC begins to produce CO before and after SSG treatment, respectively; similarly, t_2 and t_2' are the temperature points at which FC starts to generate CO before and after SSG treatment. Before undergoing SSG treatment, FC and GC begin to generate CO at temperatures of 90 °C (t_1) and 110 °C (t_2), respectively. However, after the SSG treatment, the onset temperature for CO generation in both FC and GC is significantly delayed, with values of 120 °C (t_1') and 140 °C (t_2'), respectively. This indicates that the SSG treatment effectively enhances the thermal stability of FC and GC. At the same temperature, the amount of CO generated after SSG treatment is consistently lower than that produced by raw coal. This further highlights the effectiveness of the SSG treatment in reducing the combustion reactivity and improving the safety of coal.

Fig. 11(b) shows the oxidation inhibition rate of FC and GC treated by SSG. The data clearly demonstrates that coal samples treated with SSG exhibit a significant reduction in CO production under low temperature conditions. This phenomenon can be attributed to the fact that SSG encapsulates the coal particles and fills the void spaces within the coal structure, effectively reducing the contact between oxygen and the coal (Wang et al., 2021). Table 4 provides a comparison of the crossover temperature changes in GC and FC before and after SSG treatment. In comparison to raw coal, the crossover temperature of both GC and FC increases after undergoing SSG treatment. Additionally, the time required for these coal samples to reach their respective crossover temperatures also increases. This indicates that the SSG treatment effectively enhances the thermal stability of coal, which is closely linked to the fact that SSG encapsulates the coal particles, effectively covering their surface. By doing so, it absorbs the heat generated during coal self-combustion and helps to reduce the overall surface temperature of the coal body (Huang et al., 2018).

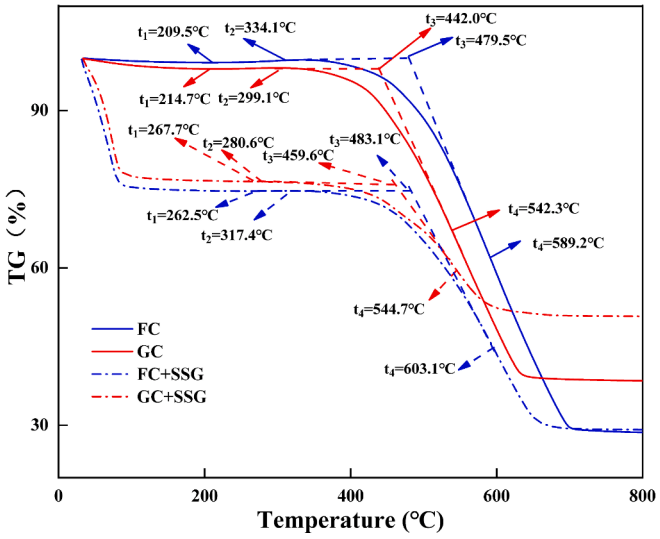

Fig. 12. TG curves of FC and GC before and after SSG treatment.

4.5. Thermal stability

Fig. 12 shows the TG curves of FC and GC before and after SSG treatment. The weight loss of coal can be generally divided into three distinct stages: the dehydration stage, the oxidative weight gain stage, and the decomposition weight loss stage (Qi et al., 2017, Huang et al., 2023). During the dehydration phase, a minor quantity of free water, adsorbed water, and structural water will vaporize as the temperature rises. Nevertheless, for the coal samples treated with SSG, owing to the abundant free water in SSG, there is a pronounced stage of weight reduction prior to reaching 100 ℃. Moreover, the starting temperature of oxidative weight gain is denoted by t_1, while the initial temperature of thermal decomposition is represented by t_2. The ignition point

Table 5
Characteristic temperatures.

Sample	Starting temperature of oxidative weight gain t_1 (℃)	Initial temperature of thermal decomposition t_2 (℃)	Ignition point temperature t_3 (℃)	Temperature with the highest weight loss rate t_4 (℃)
FC	209.5	334.1	479.5	589.2
FC+SSG	262.5	317.4	483.1	603.1
GC	214.7	299.1	442.0	542.3
GC+SSG	267.7	280.6	459.6	544.7

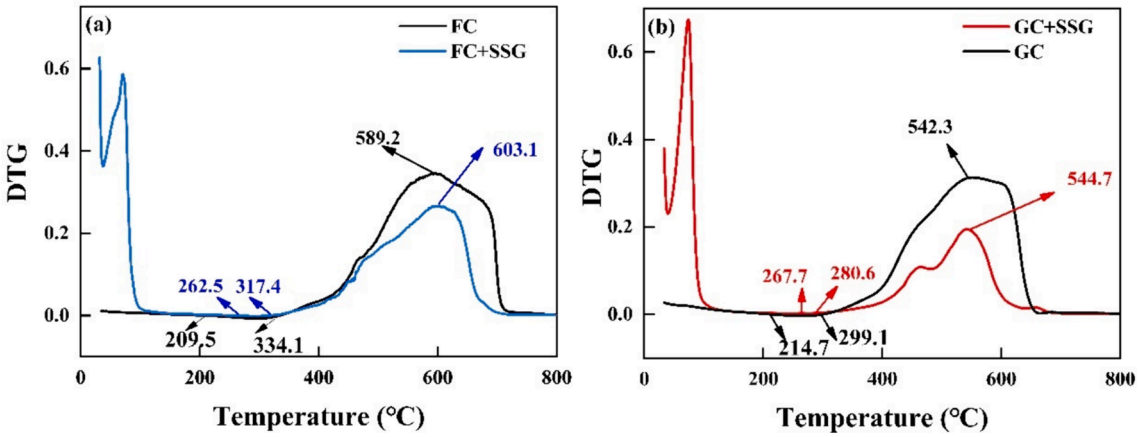

Fig. 13. DTG curves of FC and GC before and after SSG treatment (a) FC; (b) GC.

Table 6
Changes in specific surface area of FC and GC before and after SSG treatment.

Sample	Original specific surface area	Specific surface area after SSG treatment
FC	2.4	1.5
GC	7.7	7.5

temperature is identified as t_3, and the temperature with the highest weight loss rate is marked as t_4. After undergoing the necessary processing, the obtained data of t_1, t_2, t_3, and t_4 are presented in Table 5. It is evident that the low-temperature oxidative stage (t_1-t_2) for both GC and FC coal samples is affected by the SSG treatment. Specifically, the starting temperature of oxidative weight gain (t_1) and the ignition point temperature (t_3) are observed to be delayed after undergoing SSG treatment. This indicates that the SSG treatment has a positive impact on the thermal stability of coal. When SSG acts on coal, it inhibits the adsorption of oxygen by the coal particles, thereby hindering the process of coal oxygen complex weight gain. As a result, the weight gain rate increases with temperature, but it remains lower than the weight loss rate. This leads to an earlier onset of thermal decomposition, as indicated by the reduced initial temperature of thermal decomposition (t_2). Overall, the SSG treatment enhances the thermal stability of coal by delaying its oxidative weight gain and ignition point temperatures.

Fig. 13 shows the DTG curves of FC and GC before and after SSG treatment. When considering the results in Fig. 12 and Fig. 13 together, it can be observed that in the high-temperature rapid combustion stage, the temperature with the highest weight loss rate (t_4) is delayed after undergoing SSG treatment. This further highlights the positive impact of the SSG treatment on the thermal stability of coal. Furthermore, it can be observed that throughout the entire weight loss stage, the weight loss rate of the coal samples after undergoing SSG treatment is consistently lower than that of raw coals. This indicates that the SSG treatment effectively reduces the combustibility of coal and improves its safety. In both the low-temperature oxidative and high-temperature combustion stages, SSG encapsulates and fills the coal body, which helps to inhibit the reaction between coal and oxygen. This encapsulation effect of SSG plays a role in reducing the reactivity of coal and improving its safety during thermal processes.

4.6. Low temperature nitrogen adsorption experiment (LTNA)

Table 6 provides a comparison of the specific surface area changes in FC and GC before and after undergoing SSG treatment. The specific surface area of coal is an important parameter that can provide insight into its pore structure. A larger specific surface area typically indicates a greater number of contact active sites within the coal structure. This can have implications for the reactivity and combustion characteristics of coal, as it may lead to increased oxidation and combustion rates. Based on the data presented in Table 6, it can be observed that GC has a larger specific surface area than FC. This increased surface area may contribute to the higher reactivity and propensity for autoignition of GC compared to FC. Despite the initial difference in specific surface area between GC and FC, it is important to note that after undergoing SSG treatment, the specific surface area of both coal samples decreases. This indicates that the SSG treatment has a significant impact on reducing the reactivity of coal by decreasing the number of contact active sites on its surface. As a

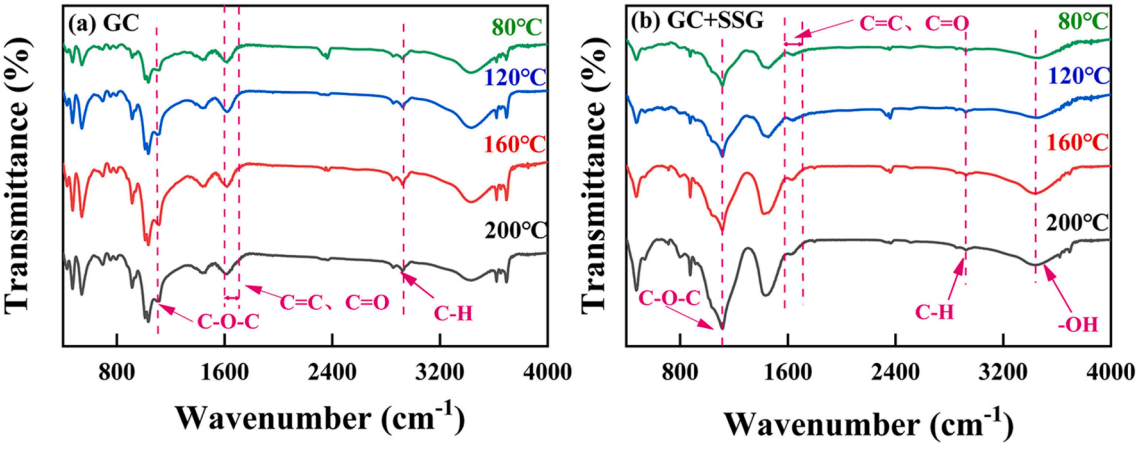

Fig. 14. FTIR analysis of GC before and after SSG treatment.

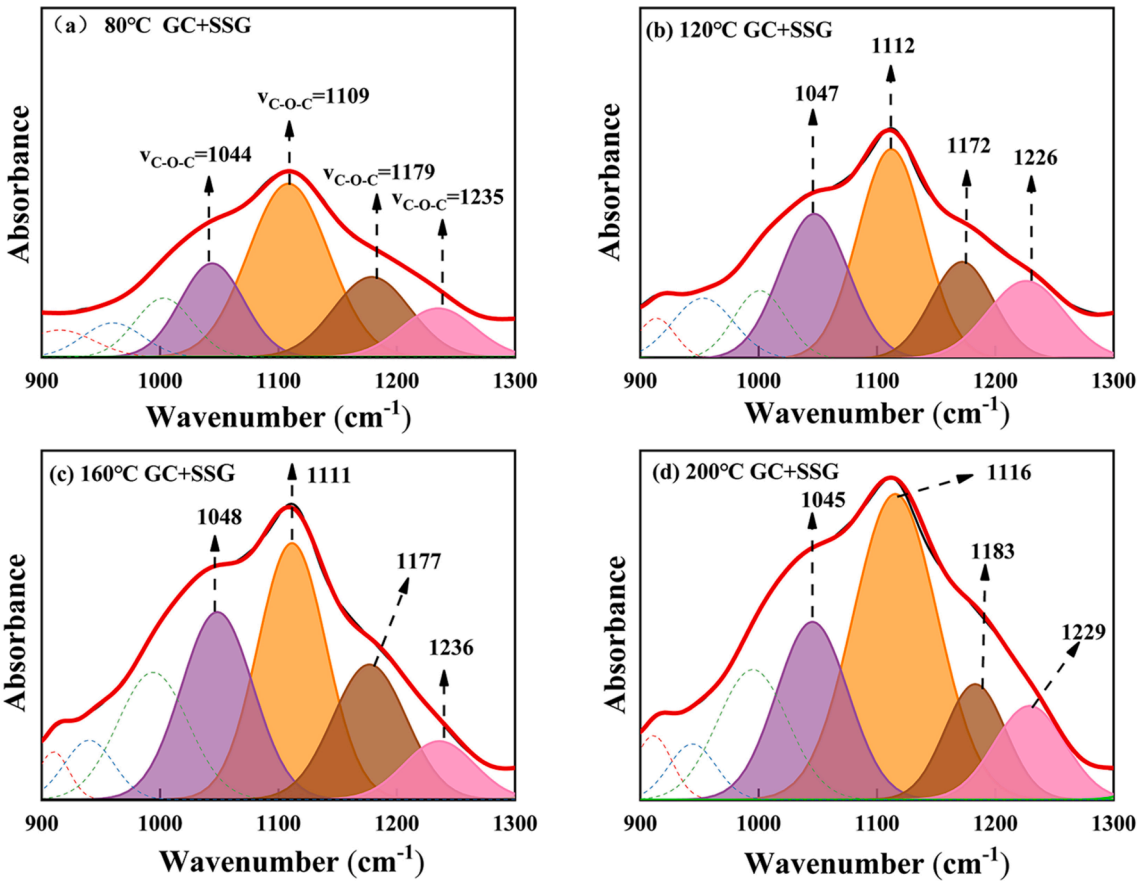

Fig. 15. C-O-C IR peak fitting of GC after SSG treatment in the range of 900–1300 cm^{-1}: (a) 80 ℃; (b) 120 ℃; (c) 160 ℃; (d) 200 ℃.

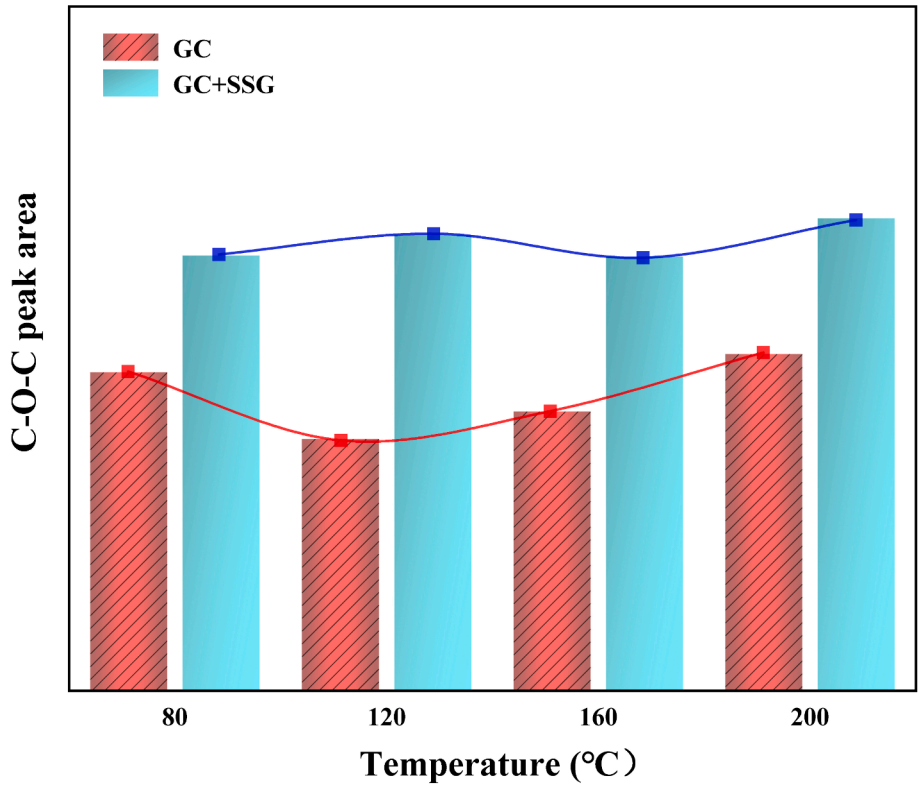

Fig. 16. Changes in the area of C-O-C absorption peaks before and after SSG treatment.

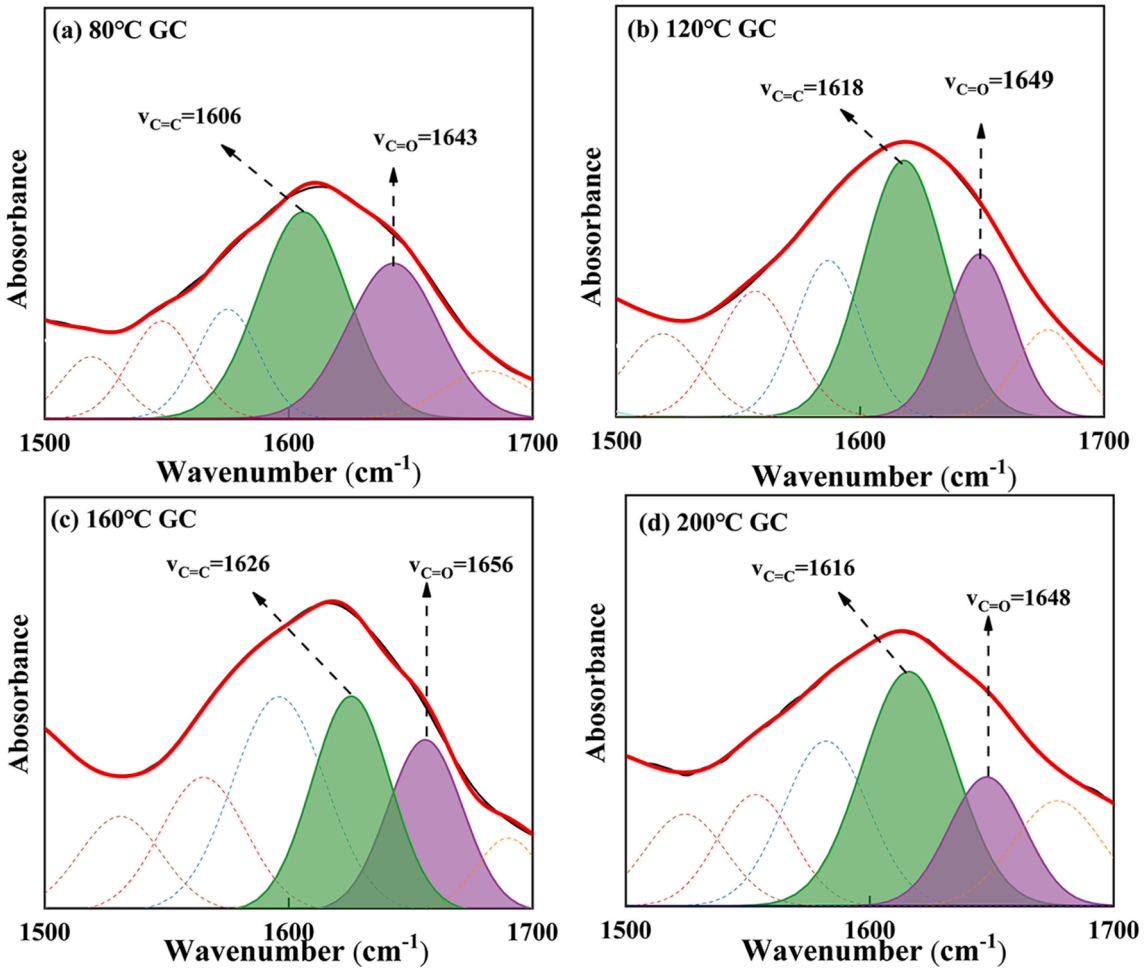

Fig. 17. C=C and C=O Infrared peaks fitting diagram of GC before SSG treatment at 1500–1700 cm^{-1}: (a) 80 ℃; (B) 120 ℃; (C) 160 ℃; (d) 200 ℃.

colloidal solution, SSG is able to surround and coat the coal particles, effectively reducing their exposure and contact with oxygen. Additionally, SSG can fill the pores within the coal structure, leading to a decrease in the overall number of pores and a consequent reduction in specific surface area. This encapsulation and filling effect of SSG helps to inhibit the reaction between coal and oxygen, which makes it less likely for spontaneous combustion to occur.

4.7. Flame retardant mechanism

4.7.1. FTIR analysis

Fig. 14 presents the infrared spectra of GC coal samples before and after undergoing SSG treatment at various temperatures. As shown in Fig. 15, the C-O-C absorption peak of GC after SSG treatment is significantly higher than that of raw GC, suggesting that there is an increase in the number of ether bonds present in the coal structure. The presence of more ether bonds can contribute to greater stability of the coal molecules, as they are known to enhance the resistance of coal to thermal decomposition and combustion (Huang et al., 2018; Zhang et al., 2020b). In addition, the –OH absorption peak of GC coal samples after undergoing SSG treatment is observed to decrease in intensity compared to that of raw GC, suggesting a decrease in the number of oxygen-containing functional groups, such as phenols and alcohols. These groups can contribute to the oxidative activity of coal, making it more prone to oxidation and combustion. Therefore, the reduction in the –OH peak after SSG treatment indicates a decrease in the oxidative activity of the coal, which can be beneficial for improving its safety and stability during thermal processes (Dou et al., 2022).

Fig. 15 and Fig. 16 present the changes in the area of C-O-C absorption peaks before and after SSG treatment for GC coal samples. It can be observed that as the temperature increases, the area of the ether bond absorption peak for GC coal samples treated with SSG is consistently higher than that of the raw GC samples, which may contribute to the enhanced resistance of the treated coal to thermal decomposition and combustion. This is because that ether bonds are known to have a higher energy barrier for breaking compared to other types of chemical bonds, such as carbon–oxygen bonds (Han et al., 2022; Lu et al., 2022a, 2022b).

Fig. 17 illustrates the infrared absorption peak fitting results for both C=C and C=O in GC, within the range of 1500–1700 cm^{-1}. The high degree of polymerization and stable structure of the C=C bond result in minimal changes throughout the oxidation process, rendering it unsuitable as an indicator for coal oxidation activity (Ma et al., 2019, Li et al., 2020). In contrast, C=O, being an oxygen-containing functional group, can not only undergo thermal decomposition to directly form carbon oxides (Formulas (1)), but also are primarily functions as a transitional group in the oxidation process of aliphatic hydrocarbons (Wang et al., 2003), eventually leading to the formation of –COO- and subsequently carbon oxides (Formulas (2) and (3)). Consequently, the C=O can be employed as a marker to analyze the oxidation reaction of coal.

$$-C=O \rightarrow -OH + CO \quad (1)$$

$$-C=O + -OH \rightarrow -COOH \quad (2)$$

$$-COOH + O_2 \rightarrow CO_2 + H_2O \quad (3)$$

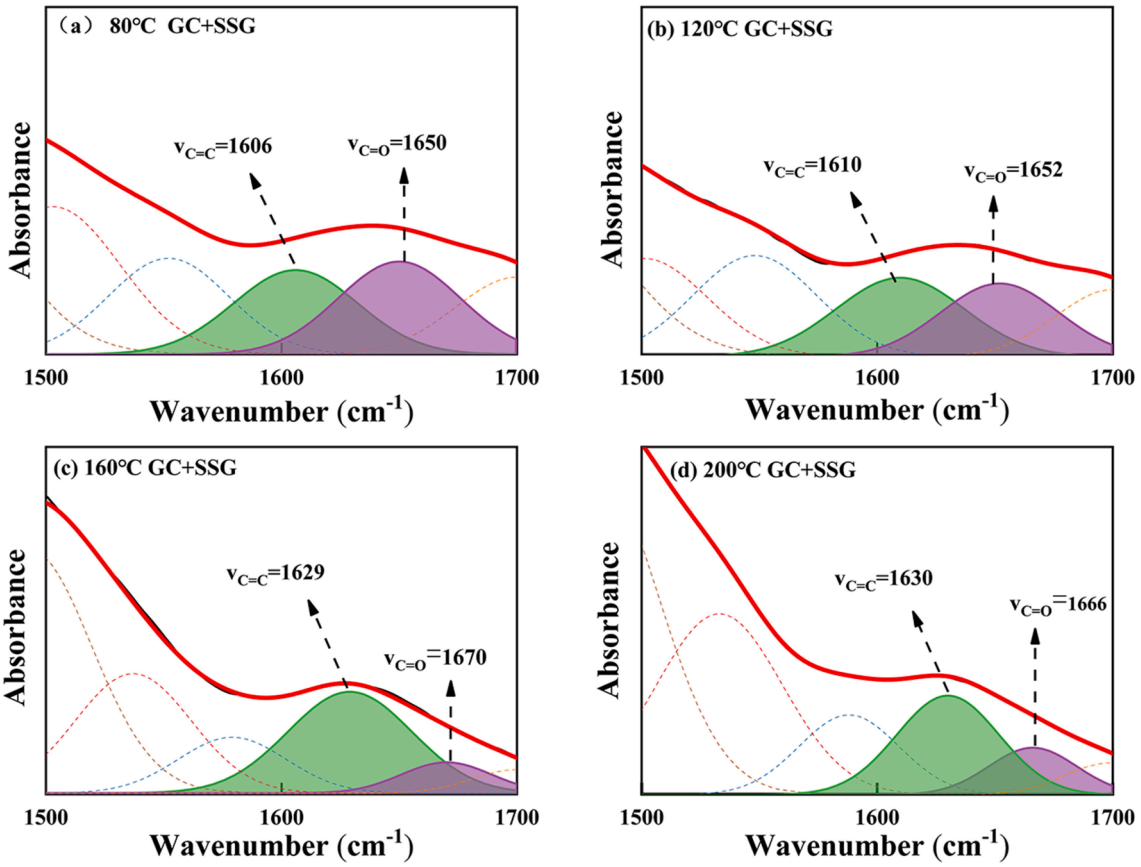

Fig. 18. C=C and C=O IR peak fitting of GC after SSG treatment in the range of 1500–1700 cm^{-1}: (a) 80 ℃; (b) 120 ℃; (c) 160 ℃; (d) 200 ℃.

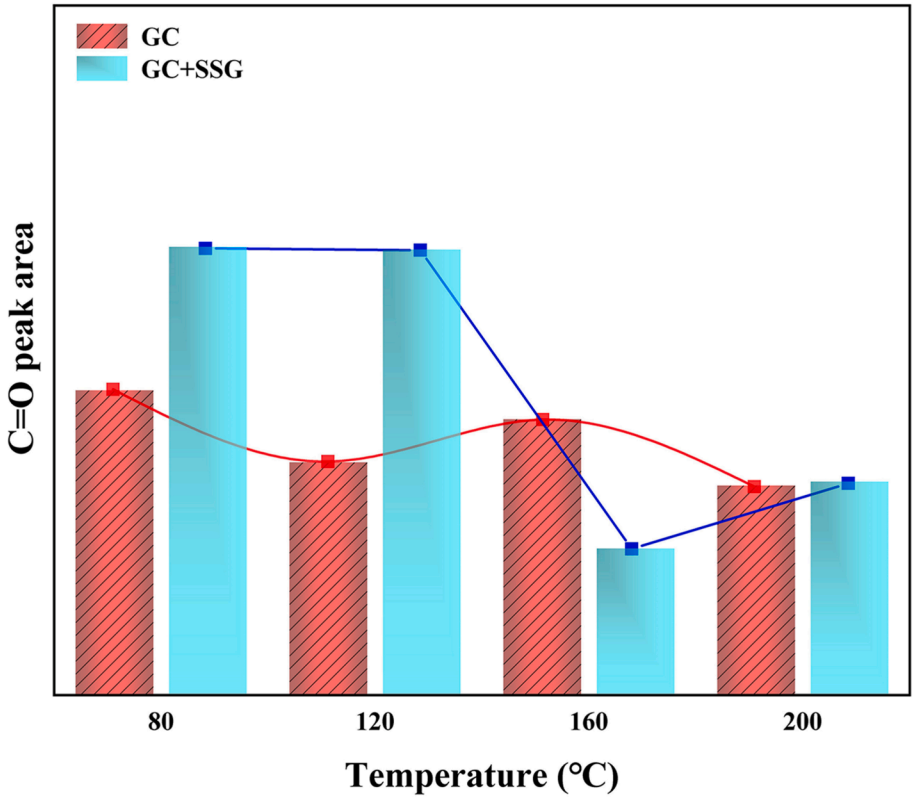

Fig. 19. Changes in the area of C=O absorption peaks before and after SSG treatment.

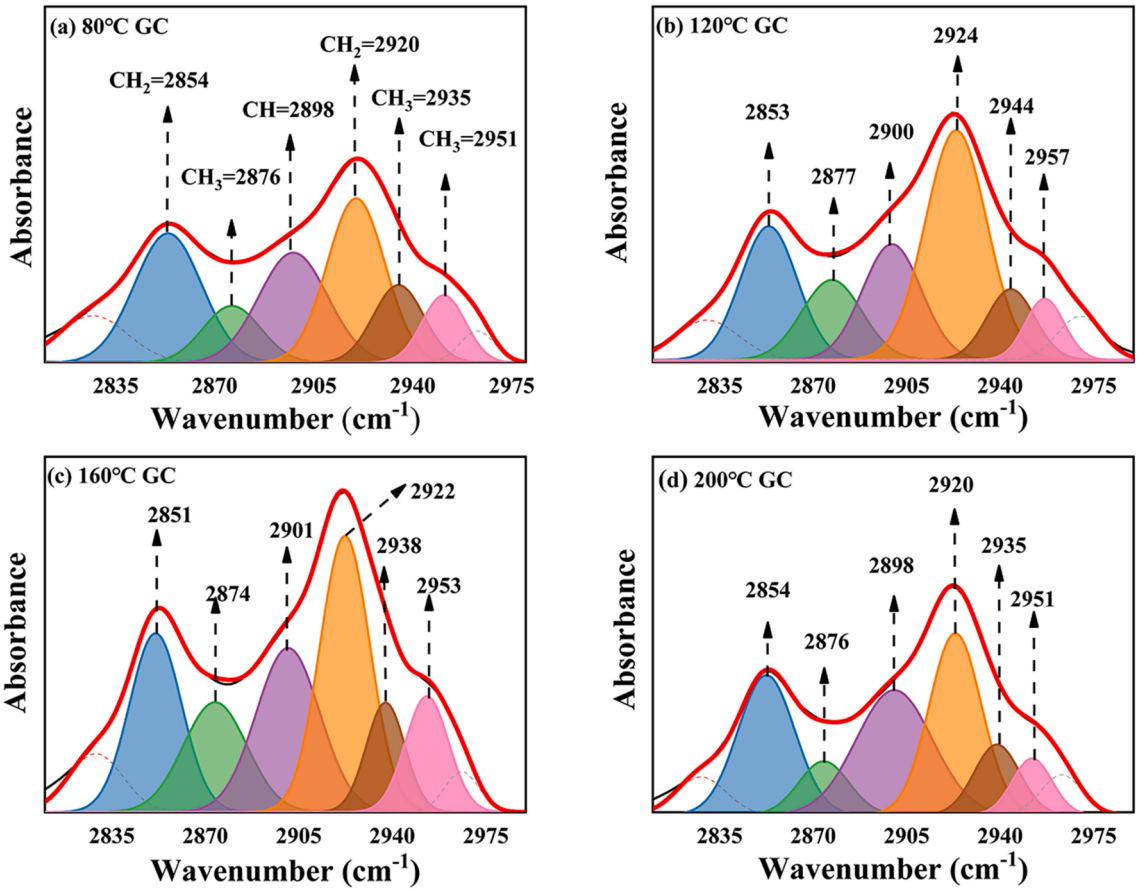

Fig. 20. IR peak fitting of $–CH_2$ and $–CH_3$ in GC before SSG treatment in the range of 2800–3000 cm^{-1}: (a) 80 ℃; (b) 120 ℃; (c) 160 ℃; (d) 200 ℃.

From Figs. 17 and 19, it can be observed that during the low-temperature oxidation stage of 80–120 °C, the C=O absorption peak area decreases. Within this temperature range, the C=O in GC gradually undergoes consumption to produce CO, as illustrated in Fig. 11 (a). Nevertheless, during the slow combustion stage of 120–160 °C, the C=O absorption peak area increases and the oxidation rate accelerates, resulting in an increase in the consumption of C=O. However, simultaneously, the $–CH_2$ and $–CH_3$ in GC also undergo accelerated oxidation, leading to the production of additional C=O (Formulas (4) and (5)). At this point, the consumption rate of C=O is lower than its production rate, causing an overall increase in the number of C=O functional groups. In the rapid combustion stage of 160–200 °C, the C=O absorption peak area decreases sharply, indicating intense combustion of GC with a consumption rate significantly greater than its production rate.

$$-CH_2 + O_2 \rightarrow -C=O + H_2O \quad (4)$$

$$-CH_3 + O_2 \rightarrow -C=O + H_2O \quad (5)$$

However, as illustrated in Figs. 18 and 19 after the SSG treatment, the peak area of C=O remains relatively stable from 80-120 °C, indicating that there is minimal decomposition of C=O during this temperature range. This observation is further supported by Fig. 11 (a), which clearly indicates that no CO is generated in the GC sample treated with SSG within the temperature range of 80–120 °C. This phenomenon may be attributed to the fact that SSG absorbs heat, thereby reducing the temperature and isolating oxygen. As a result, it helps maintain a lower internal temperature within GC before reaching 120 °C. Therefore, before 120 °C, the peak area of C=O is larger than that of the original GC (As shown in Fig. 19). As the temperature increases to 160 °C, a significant decrease in the C=O absorption peak area is observed, with the treated sample exhibiting an even lower peak area compared to the untreated GC. The action of SSG leads to a reduction in the consumption of $–CH_2$ and $–CH_3$ groups and a decrease in the generation of C=O. Additionally, the existing C=O in GC is consumed to produce CO, further contributing to a lower production rate of C=O compared to its consumption rate. However, during the intense combustion between 160–200 °C, an interesting phenomenon occurs. The peak area of C=O actually increases for the sample treated by SSG. At this stage, a significant number of $–CH_2$ and $–CH_3$ groups are consumed, leading to an increase in the production of C=O. Furthermore, the peak area of C=O in the treated sample is also higher than that of the untreated GC during this temperature range. This suggests that the consumption of C=O is lower in the treated sample, which is in line with the findings in Fig. 11 (a), where GC treated by SSG produces significantly less CO. This observation supports the notion that SSG encapsulates around GC, effectively reducing temperature and preventing oxygen from coming into direct contact with the coal.

Figs. 20 and 21 provide a fitting diagram of the $–CH_2$ and $–CH_3$ infrared peak in GC before and after treatment with SSG. Fig. 22 illustrates the variations in the area of C–H absorption peaks in GC before and after SSG treatment. As illustrated in Fig. 20, the peak areas of –CH, $–CH_2$, and $–CH_3$ increase gradually with an increase in temperature between 80–160 °C. This trend can be attributed to the fact that long-chain aliphatic hydrocarbons present in coal are susceptible to attack by oxygen molecules at these temperatures and are consequently cracked into shorter chain aliphatic hydrocarbons (Zhang et al., 2020a; Zhou et al., 2021). However, upon reaching the intense combustion stage at 160–200 °C, a noticeable reduction in the absorption peak areas of –CH, $–CH_2$, and $–CH_3$ is observed. These functional groups will not only be oxidized into other oxygen-containing functional groups, but also produce a large number of hydroxyl gases such as C_2H_4 and C_2H_6 (Zhang et al., 2020a). As depicted in Fig. 21 and Fig. 22, the overall

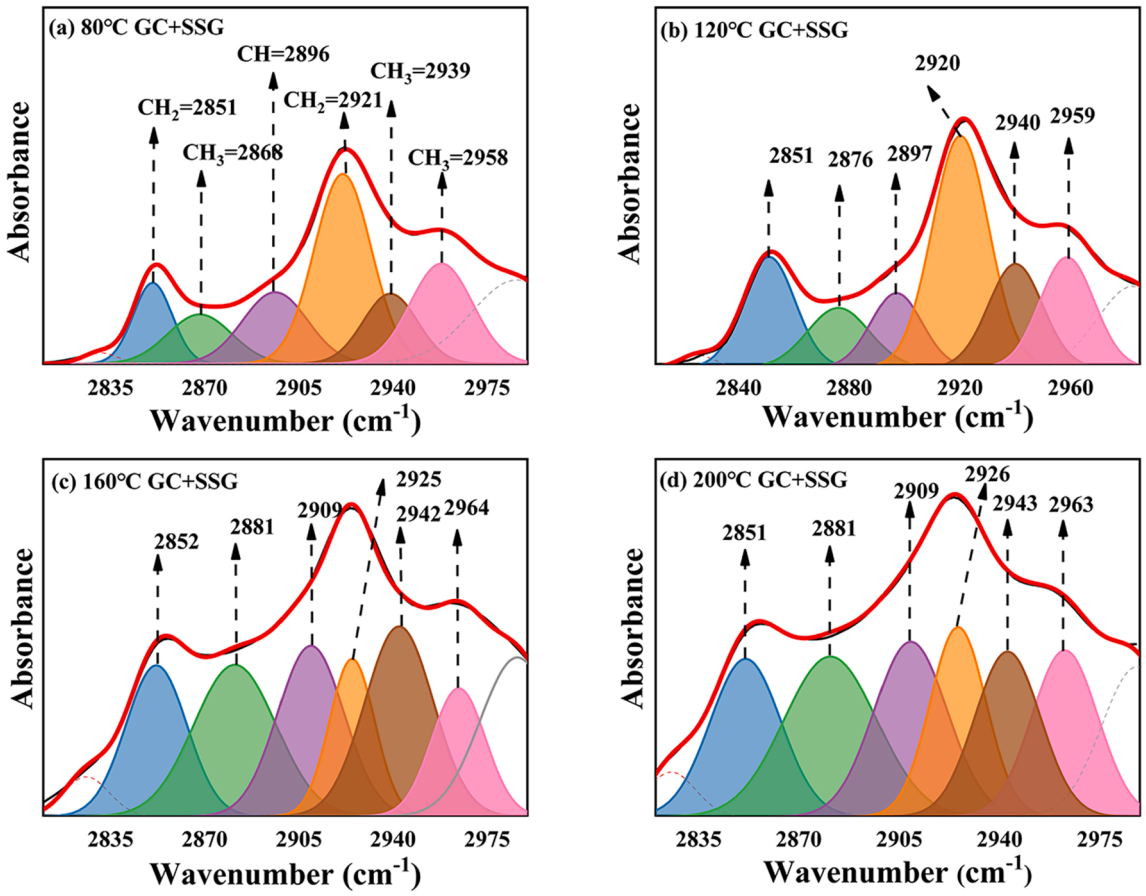

Fig. 21. IR peak fitting of $-CH_2$ and $-CH_3$ in GC after SSG treatment in the range of 2800–3000 cm^{-1}: (a) 80 ℃; (b) 120 ℃; (c) 160 ℃; (d) 200 ℃.

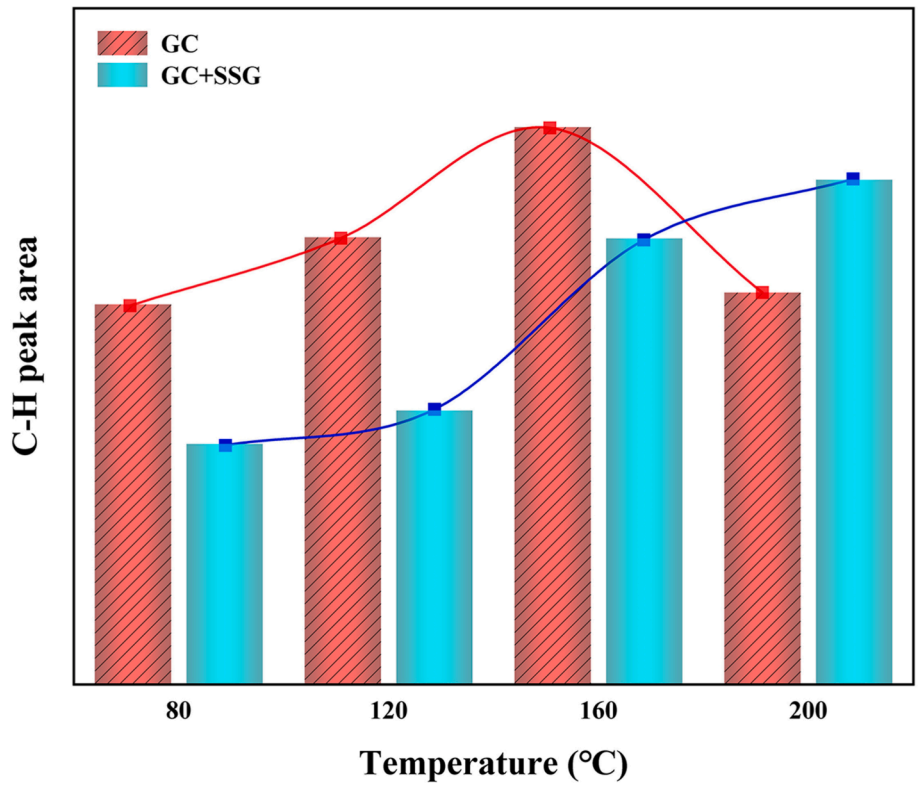

Fig. 22. Changes in the area of C–H absorption peaks before and after SSG treatment.

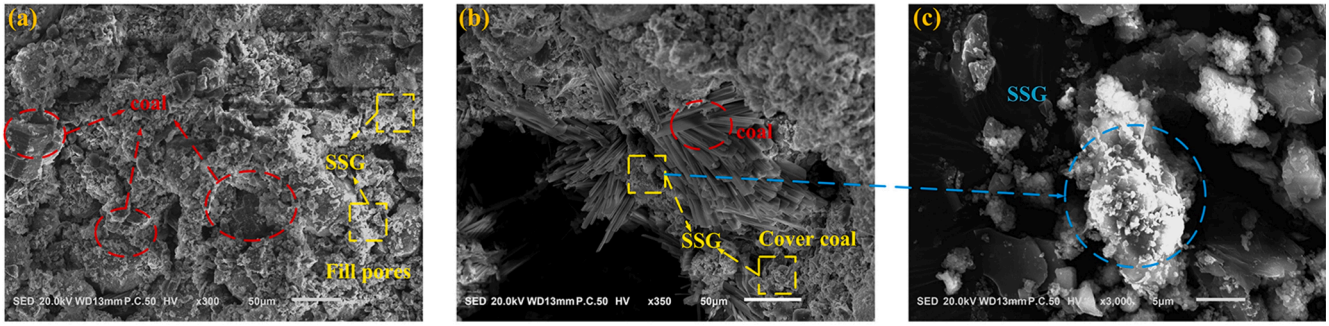

Fig. 23. SEM micrographs after SSG treatment.

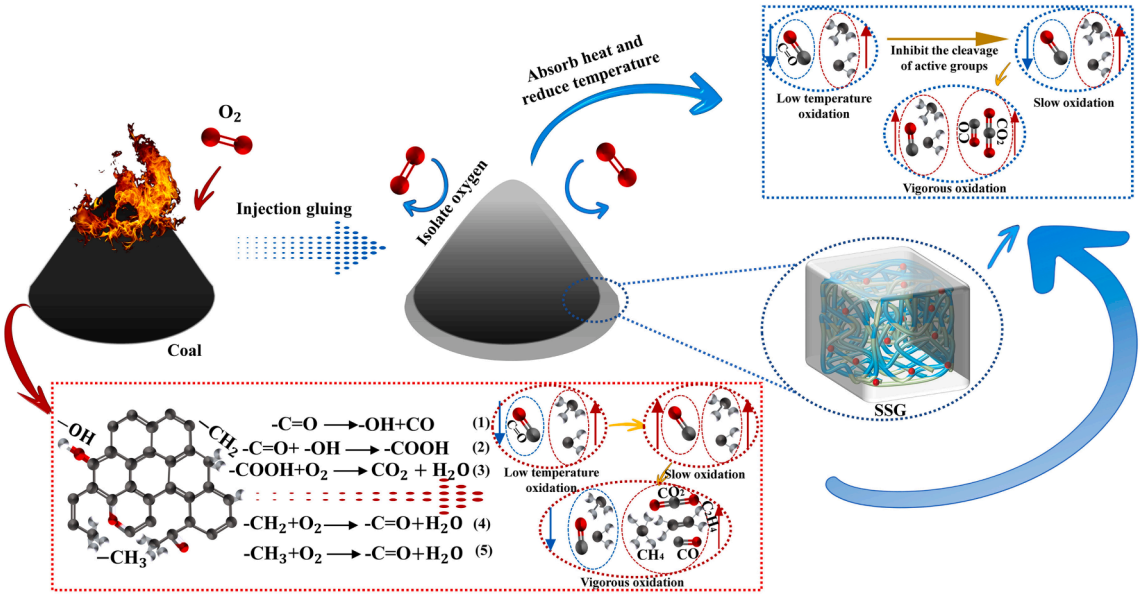

Fig. 24. Principle of fire prevention and extinguishing.

absorption peak area of –CH, –CH_2, and –CH_3 in GC after SSG treatment increases between 80 and 200 °C. However, it is worth noting that the absorption peak area before 160 °C is lower compared to that of the original GC. As the temperature rises, the long chain macromolecules present in coal undergo breakdown, resulting in the formation of more short-chain molecules. SSG plays a crucial role in this process by lowering the temperature and isolating oxygen, thereby slowing down the rate of reaction. This leads to a reduction in the production of hydroxyl groups and other related compounds. However, the peak area in GC after being treated with SSG is larger than that of the untreated GC at 200 °C. This observation implies that the GC treated with SSG does not undergo rapid combustion to produce hydrocarbon gases. In other words, at this stage, the GC treated with SSG is still primarily dominated by cracking reactions.

4.7.2. *Microscopy characterization*

Fig. 23 presents SEM images of GC after undergoing SSG treatment. In both Fig. 23(a) and (b), it is evident that upon pouring SSG onto the coal surface, a gel-like aggregate layer forms around the coal body, creating a protective covering. In Fig. 23(b), SSG also infiltrates the structural voids within the coal body, minimizing contact between coal particles and oxygen, thus isolating oxygen. Fig. 23(c) provides an enlarged view of the SSG surface, revealing that after dehydration, SSG fills the voids in the coal body in an amorphous polymer form. The microscopic electron microscope images of GC treated with SSG also indirectly confirm that SSG achieves its flame-retardant effect by enveloping the coal surface to isolate oxygen.

4.7.3. *Principle of fire prevention and extinguishing*

Fig. 24 provides a summary of the fire prevention and extinguishing principles of SSG. On one hand, the injection of SSG can help to isolate oxygen. The SSG colloid transforms the gas–solid interface, where coal comes into contact with oxygen, into a gas–liquid-solid interface. This transformation prevents oxygen molecules from colliding with active groups in coal, thereby reducing the formation of oxygen-containing functional groups and inhibiting coal oxidation. On the other hand, SSG itself possesses excellent water retention properties and contains a significant amount of water. The SSG colloid is fixed around the coal body, absorbing heat and cooling it down, thereby inhibiting the increase in coal body temperature. This process prolongs the time of low-temperature oxidation of coal, hinders the breaking of long-chain aliphatic hydrocarbons, slows down the generation rate of active groups, and prevents violent combustion of the coal body.

5. Conclusion

The steel slag-based fire prevention and extinguishing composite gel can be synthesized under the activation condition of 1.5 M sodium silicate, exhibiting a short gel time and low water loss rate. And a stable gel structure is formed in this gel through the hydrolysis reaction and geopolymerization reaction. In this structure, C-S-H, C-A-S-H, and geopolymer are interconnected and adhered, providing excellent fire

prevention and extinguishing capabilities.

After the injection of SSG into gas coal and fat coal, the temperature required for CO production is increased by 30 °C, and the time taken for gas coal to reach the crossover temperature is prolonged by 51 min. Furthermore, the weight loss rate of coal is significantly reduced, and the contact area between coal and oxygen is diminished. On the one hand, SSG wraps around and fills the cracks inside the coal body, reducing the specific surface area of the coal and effectively isolating the contact between oxygen and the coal's active groups, thereby hindering their reaction. On the other hand, SSG possesses excellent water retention capabilities, which allows it to absorb heat and reduce temperature while covering the coal body. Additionally, SSG inhibits the generation of active groups in coal, making the internal structure more stable and less prone to breaking.

CRediT authorship contribution statement

Tan Li: Writing – review & editing, Writing – original draft, Visualization, Conceptualization. **Hengze Zhao:** Validation, Supervision, Methodology, Funding acquisition. **Yipei Qi:** Validation, Supervision. **Yu Zhang:** Validation, Supervision, Conceptualization. **Ye Li:** Writing – review & editing, Validation, Supervision, Resources, Funding acquisition.

Declaration of competing interest

The authors declare that they have no known competing financial interests or personal relationships that could have appeared to influence the work reported in this paper.

Acknowledgments

The authors acknowledge gratefully the financial supports from the Natural Science Foundation of Hebei Province (E2022209101, E2020209038) and the Central Government Guide for Local Scientific and Technological Development Fund (236Z7603G).

References

Bernal, S.A., Mejía de Gutiérrez, R., Provis, J.L., 2012. Engineering and durability properties of concretes based on alkali-activated granulated blast furnace slag/metakaolin blends. Constr. Build. Mater. 33, 99–108. https://doi.org/10.1016/j.conbuildmat.2012.01.017.

Dou, G., Liu, J., Jiang, Z., et al., 2022. Preparation and characterization of a lignin based hydrogel inhibitor on coal spontaneous combustion. Fuel 308. https://doi.org/10.1016/j.fuel.2021.122074.

Duan, S., Liao, H., Cheng, F., et al., 2018. Investigation into the synergistic effects in hydrated gelling systems containing fly ash, desulfurization gypsum and steel slag. Constr. Build. Mater. 187, 1113–1120. https://doi.org/10.1016/j.conbuildmat.2018.07.241.

Guo, J., Bao, Y., Wang, M., 2018. Steel slag in China: Treatment, recycling, and management. Waste Manag. 78, 318–330. https://doi.org/10.1016/j.wasman.2018.04.045.

Guo, J., Cai, G., Jin, Y., et al., 2020. An Improved Composite Fly Ash Gel to Extinguish Underground Coal Fire in Close Distance Coal Seams: A Case Study. Adv. Mater. Sci. Eng. 2020, 1–11. https://doi.org/10.1155/2020/5695471.

Guo, X., Pan, X., 2020. Effects of Steel Slag on Mechanical Properties and Mechanism of Fly Ash-Based Geopolymer. J. Mater. Civ. Eng. 32 https://doi.org/10.1061/(asce)mt.1943-5533.0003012.

Han, C., Nie, S., Liu, Z., et al., 2022. A Novel Highly Stable Biomass Gel Foam Based on Double Cross-Linked Structure for Inhibiting Coal Spontaneous Combustion. Energies 15. https://doi.org/10.3390/en15145207.

Huang, Z., Sun, C., Gao, Y., et al., 2018. R&D of colloid components of composite material for fire prevention and extinguishing and an investigation of its performance. Process Saf. Environ. Prot. 113, 357–368. https://doi.org/10.1016/j.psep.2017.11.004.

Huang, Z., Wang, G., Ding, H., et al., 2023. Study on the inhibition performance of double network physicochemical nanocomposite gel inhibitor on coal spontaneous combustion. Fuel 350. https://doi.org/10.1016/j.fuel.2023.128697.

Jiang, Y., Ling, T.-C., Shi, C., et al., 2018. Characteristics of steel slags and their use in cement and concrete—A review. Resour. Conserv. Recycl. 136, 187–197. https://doi.org/10.1016/j.resconrec.2018.04.023.

Jing, W., Jiang, J., Ding, S., et al., 2020. Hydration and Microstructure of Steel Slag as Cementitious Material and Fine Aggregate in Mortar. Molecules 25. https://doi.org/10.3390/molecules25194456.

Li, Y., Hu, X., Cheng, W., et al., 2020. A novel high-toughness, organic/inorganic double-network fire-retardant gel for coal-seam with high ground temperature. Fuel 263. https://doi.org/10.1016/j.fuel.2019.116779.

Li, S., Zhou, G., Wang, Y., et al., 2019. Synthesis and characteristics of fire extinguishing gel with high water absorption for coal mines. Process Saf. Environ. Prot. 125, 207–218. https://doi.org/10.1016/j.psep.2019.03.022.

Liu, J., Guo, R., 2018. Applications of Steel Slag Powder and Steel Slag Aggregate in Ultra-High Performance Concrete. Advances in Civil Engineering. 2018, 1–8. https://doi.org/10.1155/2018/1426037.

Liu, H., He, H., Li, Y., et al., 2021. Coupling effect of steel slag in preparation of calcium-containing geopolymers with spent fluid catalytic cracking (FCC) catalyst. Constr. Build. Mater. 290 https://doi.org/10.1016/j.conbuildmat.2021.123194.

Liu, Y., Liu, M., Li, H., et al., 2023. Hydration kinetics of Portland cement shifting from silicate to aluminate dominance based on multi-mineral reactions and interactions. Mater. Des. 233 https://doi.org/10.1016/j.matdes.2023.112228.

Liu, Z., Zhang, D.-W., Li, L., et al., 2019. Microstructure and phase evolution of alkali-activated steel slag during early age. Constr. Build. Mater. 204, 158–165. https://doi.org/10.1016/j.conbuildmat.2019.01.213.

Lu, W., Sun, X., Gao, L., et al., 2022a. Study on the characteristics and mechanism of DL-malic acid in inhibiting spontaneous combustion of lignite and bituminous coal. Fuel 308. https://doi.org/10.1016/j.fuel.2021.122012.

Lu, W., Zhang, H., Qi, G., et al., 2022b. Synthesis and properties of environmentally friendly double-network fire fighting gel: Based on natural polymer/industrial solid waste. J. Appl. Polym. Sci. 139 https://doi.org/10.1002/app.53111.

Ma, L., Wang, D., Kang, W., et al., 2019. Comparison of the staged inhibitory effects of two ionic liquids on spontaneous combustion of coal based on in situ FTIR and micro-calorimetric kinetic analyses. Process Saf. Environ. Prot. 121, 326–337. https://doi.org/10.1016/j.psep.2018.11.008.

Mengxiao, S., Qiang, W., Zhikai, Z., 2015. Comparison of the properties between high-volume fly ash concrete and high-volume steel slag concrete under temperature matching curing condition. Constr. Build. Mater. 98, 649–655. https://doi.org/10.1016/j.conbuildmat.2015.08.134.

Onifade, M., Genc, B., Bada, S., 2020. Spontaneous combustion liability between coal seams: A thermogravimetric study. Int. J. Min. Sci. Technol. 30, 691–698. https://doi.org/10.1016/j.ijmst.2020.03.006.

Popovics, S., 1993. Portland Cement-Fly Ash-Silica Fume Systems in Concrete. Advn Cem Bas Mat. 1, 83–91.

Qi, X., Li, Q., Zhang, H., et al., 2017. Thermodynamic characteristics of coal reaction under low oxygen concentration conditions. J. Energy Inst. 90, 544–555. https://doi.org/10.1016/j.joei.2016.05.007.

Qin, B., Wang, H., Yang, J., et al., 2016. Large-area goaf fires: a numerical method for locating high-temperature zones and assessing the effect of liquid nitrogen fire control. Environ. Earth Sci. 75 https://doi.org/10.1007/s12665-016-6173-5.

Ren, X., Hu, X., Cheng, W., et al., 2020. Study of resource utilization and fire prevention characteristics of a novel gel formulated from coal mine sludge (MS). Fuel 267. https://doi.org/10.1016/j.fuel.2020.117261.

Richardson, I.G., 1999. The nature of C-S-H in hardened cements. Cem. Concr. Res. 29, 1131–1147.

Samchenko, S.V., Korshunov, A.V., 2023. Features of the formation of crystalline hydrosulfoaluminates during hydration of stoichiometric mixtures of calcium aluminates with calcium sulfate. Constr. Build. Mater. 393 https://doi.org/10.1016/j.conbuildmat.2023.132102.

Sang, M., Zhao, H., Li, Y., et al., 2024. Preparation of a Porous Geopolymer (SPG) to be Used as an Adsorbent for Cu2+ Removal. Langmuir 40, 8851–8861. https://doi.org/10.1021/acs.langmuir.3c04013.

Shi, X., Zhang, Y., Chen, X., et al., 2021. Effects of thermal boundary conditions on spontaneous combustion of coal under temperature-programmed conditions. Fuel 295. https://doi.org/10.1016/j.fuel.2021.120591.

Slovák, V., Taraba, B., 2012. Urea and CaCl2 as inhibitors of coal low-temperature oxidation. J. Therm. Anal. Calorim. 110, 363–367. https://doi.org/10.1007/s10973-012-2482-4.

Song, J.-J., Deng, J., Zhao, J.-Y., et al., 2021. Comparative analysis of exothermic behaviour of fresh and weathered coal during low-temperature oxidation. Fuel 289. https://doi.org/10.1016/j.fuel.2020.119942.

Song, W., Zhu, Z., Pu, S., et al., 2020. Efficient use of steel slag in alkali-activated fly ash-steel slag-ground granulated blast furnace slag ternary blends. Constr. Build. Mater. 259 https://doi.org/10.1016/j.conbuildmat.2020.119814.

Tang, X., Zhao, H., Ding, H., et al., 2024. A fireproof insulation block with three-dimensional pore structure fabricated using alkali activated steel slag. Constr. Build. Mater. 425 https://doi.org/10.1016/j.conbuildmat.2024.136134.

Wang, H., Dlugogorski, B.Z., Kennedy, E.M., 2003. Analysis of the mechanism of the low-temperature oxidation of coal. Combust. Flame 134, 107–117. https://doi.org/10.1016/s0010-2180(03)00086-5.

Wang, L., Liu, Z., Yang, H., et al., 2021. A novel biomass thermoresponsive konjac glucomannan composite gel developed to control the coal spontaneous combustion: Fire prevention and extinguishing properties. Fuel 306. https://doi.org/10.1016/j.fuel.2021.121757.

Wang, S., Peng, X., Geng, J., et al., 2014. Synthesis of calcium silicate hydrate based on steel slag with various alkalinities. Journal of Wuhan University of Technology-Mater. Sci. Ed. 29, 789–794. https://doi.org/10.1007/s11595-014-0998-0.

Wang, Q., Wang, D., Zhuang, S., 2017. The soundness of steel slag with different free CaO and MgO contents. Constr. Build. Mater. 151, 138–146. https://doi.org/10.1016/j.conbuildmat.2017.06.077.

Xu, Q., Yang, S., Yang, W., et al., 2020. Micro-structure of crushed coal with different metamorphic degrees and its low-temperature oxidation. Process Saf. Environ. Prot. 140, 330–338. https://doi.org/10.1016/j.psep.2020.05.007.

Xue, D., Hu, X., Cheng, W., et al., 2020. Carbon dioxide sealing-based inhibition of coal spontaneous combustion: A temperature-sensitive micro-encapsulated fire-retardant foamed gel. Fuel 266. https://doi.org/10.1016/j.fuel.2020.117036.

Yu, M., Yang, N., Liu, Z., et al., 2023. Experimental preparation and mechanism analysis of a neotype composite gel for coal spontaneous combustion prevention and coal-fire extinguishment. Fuel 339. https://doi.org/10.1016/j.fuel.2023.127448.

Zhang, Y., Hou, Y., Zhao, J., et al., 2020a. Heat Release Characteristic of Key Functional Groups during Low-Temperature Oxidation of Coal. Combust. Sci. Technol. 193, 2692–2703. https://doi.org/10.1080/00102202.2020.1755970.

Zhang, L., Shi, B., Qin, B., et al., 2017. Characteristics of Foamed Gel for Coal Spontaneous Combustion Prevention and Control. Combust. Sci. Technol. 189, 980–990. https://doi.org/10.1080/00102202.2016.1264942.

Zhang, S., Wu, B., Ren, Y., et al., 2023. The Preparation Process and Hydration Mechanism of Steel Slag-Based Ultra-Fine Tailing Cementitious Filler. Gels. 9 https://doi.org/10.3390/gels9020082.

Zhang, Y., Xu, J., Wang, D., 2020b. Experimental Study on the Inhibition Effects of Nitrogen and Carbon Dioxide on Coal Spontaneous Combustion. Energies 13. https://doi.org/10.3390/en13205256.

Zhao, J., Wang, W., Fu, P., et al., 2021. Evaluation of the spontaneous combustion of soaked coal based on a temperature-programmed test system and in-situ FTIR. Fuel 294. https://doi.org/10.1016/j.fuel.2021.120583.

Zhao, J., Li, Z., Wang, D., et al., 2023. Hydration superposition effect and mechanism of steel slag powder and granulated blast furnace slag powder. Constr. Build. Mater. 366 https://doi.org/10.1016/j.conbuildmat.2022.130101.

Zhou, F., Ren, W., Wang, D., et al., 2006. Application of three-phase foam to fight an extraordinarily serious coal mine fire. Int. J. Coal Geol. 67, 95–100. https://doi.org/10.1016/j.coal.2005.09.006.

Zhou, B., Yang, S., Jiang, X., et al., 2021. The reaction of free radicals and functional groups during coal oxidation at low temperature under different oxygen concentrations. Process Saf. Environ. Prot. 150, 148–156. https://doi.org/10.1016/j.psep.2021.04.007.

Zhuang, S., Wang, Q., 2021. Inhibition mechanisms of steel slag on the early-age hydration of cement. Cem. Concr. Res. 140 https://doi.org/10.1016/j.cemconres.2020.106283.